Chemosphere 339 (2023) 139605

Contents lists available at ScienceDirect

Chemosphere

journal homepage: www.elsevier.com/locate/chemosphere

Integrating thermodynamics and mathematical modelling to investigate the stoichiometry and kinetics of sulphide oxidation-nitrate reduction with a special focus on partial autotrophic denitrification

Eric Valdés [a], David Gabriel [a,*], Daniel González [a], Giulio Munz [b], Cecilia Polizzi [b]

[a] GENOCOV Research Group, Department of Chemical, Biological and Environmental Engineering, Escola d'Enginyeria, Universitat Autònoma de Barcelona, 08193, Bellaterra, Spain
[b] Department of Civil and Environmental Engineering, University of Florence, Via di S. Marta, 3, 50139, Firenze, Italy

HIGHLIGHTS

- Thermodynamics agree with theory under the high energy dissipation hypothesis.
- Five kinetic models on SO-NR processes were compared to describe PAD performance.
- Satisfactory capacity to simulate nitrite accumulation for 3 out of the 5 models.
- NO_2^- accumulation well modelled through Monod and Haldane kinetics for NO_2^- uptake.
- Haldane showed higher parametric identifiability allowing for further model simplification.

GRAPHICAL ABSTRACT

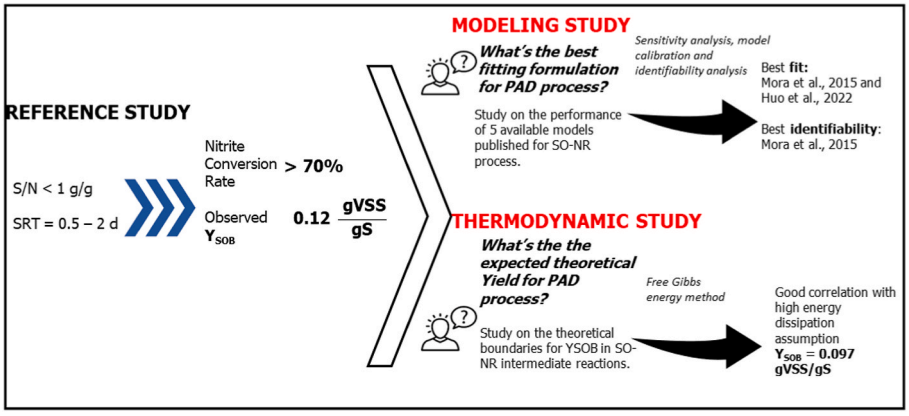

ARTICLE INFO

Handling Editor: Y Liu

Keywords:
Partial autotrophic denitrification
Nitrite accumulation
SOB
Thermodynamics
Modelling

ABSTRACT

In the present study, the stoichiometry of the Sulphur Oxidizing-Nitrate Reducing (SO-NR) process, with a focus on Partial Autotrophic Denitrification (PAD), has been evaluated through a thermodynamic-based study whereas a model-based approach has been adopted to assess process kinetics. Experimental data on process performance and biomass yields were available from a previous work achieving efficient PAD, where a biomass yield of 0.113 gVSS/gS was estimated. First, the free Gibbs energy dissipation method has been implemented, in order to provide a theoretical framework exploring the boundaries for sulphur oxidizing biomass yields. Second, a screening of available mathematical models describing SO-NR process was conducted and five published models were selected, in order to assess the most suitable model structure for describing the observed PAD kinetics. To the best of our knowledge, none of reported biomass yields are estimated in systems operating PAD as the main process and, analogously, none of the proposed models have been applied to case studies aiming at partial denitrification only. The work showed that the very low biomass yield of 0.117 ± 0.007 gVSS/gS, observed in a PAD system in our previous work, suggests that the conditions applied to achieve partial denitrification resulted

* Corresponding author. Escola d'Enginyeria, Universitat Autònoma de Barcelona, 08193, Bellaterra, Spain.
E-mail address: David.Gabriel@uab.cat (D. Gabriel).

https://doi.org/10.1016/j.chemosphere.2023.139605
Received 24 April 2023; Received in revised form 18 July 2023; Accepted 19 July 2023
Available online 22 July 2023

in a high energy-dissipating metabolism compared to complete denitrification applications. Models' analysis revealed that nitrite accumulation can be described by a classical Monod kinetics if different μ_{max} are adopted for each intermediate reaction, with Theil Inequality Coefficient values lower than 0.21 for both NO_3^- and NO_2^-. Nonetheless, adopting Haldane-type kinetics for nitrite uptake inferred higher identifiability to the model structure, resulting in confidence intervals below ±10% for all the parametric estimations. The thermodynamic and modelling outcomes support the experimental results obtained in the reference study and the critical comparison of model suitability to represent PAD process is believed pivotal to pave the way to its real-scale implementation.

1. Introduction

Sulphur Oxidation-Nitrate Reduction (SO-NR) is a complex process carried out by Sulphur Oxidizing Bacteria (SOB) and characterized by peculiar aspects such as: (i) multistep reactions involved both for electron acceptor reduction and electron donor oxidation; (ii) high chemical reactivity of reduced sulphur compounds, such as sulphide and thiosulphate; (iii) variety in microbial population able to mediate SO-NR reactions, from strictly to facultative anaerobic and from chemolithotrophic to mixotrophic cultures (Madigan et al., 2019), being *Thiobacillus* and *Sulfurimonas* the most abundant and dominant genera in aerobic and anoxic sulphur oxidation applications (Mora et al., 2014). Both sulphide oxidation and nitrate reduction are typically described as two-step processes, resulting in the possible combination of electron acceptor/electron donors described in equations (1)–(4) (see Table S2 for the solved catabolic reactions) even though the actual reactions involve several other intermediates.

$$HS^- + NO_3^- + H^+ \rightarrow S^0 + NO_2^- + H_2O \quad \text{Eq. (1)}$$

$$HS^- + 0.67\,NO_2^- + 1.67\,H^+ \rightarrow S^0 + 0.335N_2 + 1.335H_2O \quad \text{Eq. (2)}$$

$$S^0 + 3\,NO_3^- + H_2O \rightarrow SO_4^{2-} + 3\,NO_2^- + 2\,H^+ \quad \text{Eq. (3)}$$

$$S^0 + 2\,NO_2^- \rightarrow SO_4^{2-} + N_2 \quad \text{Eq. (4)}$$

In the last decades, the SO-NR process has received increasing attention as a sustainable solution to effectively remove nitrogen from streams with a low C/N ratio. Thus, it has been successfully applied in treating groundwater, secondary effluent of municipal wastewater, drinking water, mariculture wastewater (Wang et al., 2023), municipal tailwater (Li et al., 2023) and landfill leachate (Zhang et al., 2023). Furthermore, the coupling of this process with C removal has been successfully implemented in full scale facilities (SANI® process, Wu et al., 2016), as well as H_2S removal from gaseous streams such as biogas (Baspinar et al., 2011). More recently, innovative solutions are promoting the integration of gaseous and wastewater biological treatments, such as the integrated nitrogen and sulphur removal combining the anammox process and the sulphide-driven partial autotrophic denitrification, PAD (Chen et al., 2019). Such an integrated process can offer an appealing application in the treatment of wastewater side-streams generated by anaerobic digestion, typically highly rich in reduced forms of nitrogen, as well as in the H_2S removal from biogas. Even though successful PAD has been presented in recent studies using elemental sulphur, thiosulphate or sulphide as electron donor (Chen et al., 2018; Deng et al., 2022; Polizzi et al., 2022), the comprehension of the mechanism underlying successful nitrite accumulation and the consequent operational strategies to be applied are still object of discussion.

The complexity of SO-NR process is reflected in the different, and sometimes contradictory, results that can be found in the literature on the favoured electron acceptor between nitrate and nitrite as well as the observed biomass yields. For instance, some authors indicate nitrate as the preferred electron acceptor when coupled with sulphide oxidation (Campos et al., 2008; Guo et al., 2016), whereas other works report nitrite instead (Cui et al., 2019). Biomass cultivation mode (e.g., suspended or granular systems), operational conditions (e.g. SRT, S/N ratio) and biomass adaptation also affect observed uptake rates and stoichiometry. SOB biomass yields are reported in the range of 0.1–0.4 gVSS/gS (see Polizzi et al., 2022). Due to the complexity of the possible reaction combinations, solving the full stoichiometry is not a trivial exercise (Klatt and Polerecky, 2015). When dealing with complex processes, mathematical models are an effective tool for gaining insight into the mechanisms underlying processes' response under different operational conditions. The models proposed in the literature for the description of SO-NR process mainly differ for the following characteristics: (1) one or two-step reactions are presented for the oxidation and reduction semi-reactions; (2) Monod kinetics are typically assumed for NO_3^- and S^0 uptake while both Monod or Haldane kinetics are encountered for HS^- and NO_2^- uptake; (3) switch functions are sometimes included in order to elicit the preferred uptake of one electron acceptor (or donor) or the other, in case multistep reactions; (4) kinetic parameters, in terms of maximum growth rate and/or half saturation coefficients, are either assumed having the same value in all reaction steps or different values for each reaction step. As a consequence, the complexity and the consequent number of parameters required by models can vary significantly.

In the present work, an integrated approach based on a thermodynamic study and mathematical modelling is proposed to gain insight, respectively, on the stoichiometry and kinetics of SO-NR, with special focus on the novel process of PAD. The work by (Polizzi et al., 2022) is selected as the reference study for successful PAD implementation. The first aim of the work is to present a theoretical framework for the biomass yields through a thermodynamic study, offering a critical comparison with experimental stoichiometric values observed in the literature on SO-NR systems as well as those estimated in the reference study on PAD. The second purpose is to achieve a mathematical representation of the observed nitrite accumulation kinetics: five models available in the literature were selected and studied through a sensitivity and identifiability analyses, in order to assess their suitability for the representation of the observed data. To the best of our knowledge, none of the reported biomass yield is estimated in a system operating PAD as the main process and, analogously, none of the proposed models have been applied to case studies aiming at representing partial denitrification only.

2. Material and methods

2.1. Experimental dataset

Data from (Polizzi et al., 2022) were considered both for the thermodynamics and modelling tasks. In the mentioned publication, successful partial denitrification (i.e., nitrite accumulation) was achieved in a chemostat under sulphide-limiting conditions. During stable operation, three operational phases were tests adopting SRT values in the range of 13–44 h and influent S/N within 0.65 and 0.95 gS/gN. Nitrite conversion rate, calculated as the nitrite production over the removed nitrate, was above 70% at all the applied conditions, with peaks close to 100%. The observed biomass yield was estimated at 0.117 ± 0.007 mgVSS/mgS. Microbial community analysis revealed that a clear population shift occurred: *Sulfurimonas* was the dominant genus in the inoculum (97% of relative abundance) and was almost completely

replaced by *Thiobacillus* (83% of relative abundance) after 80 days of operation. As reported in the work, S^0 was not measured but rather estimated, with a 10–30% error on S mass balance, depending on the operational phase. In Table S1 of the supplementary material, the main operational conditions are summarized for each phase. For the modelling purpose, phase 1a was removed from the experimental dataset since the system had not reached stable conditions.

2.2. Thermodynamic study

The free Gibbs energy dissipation method formulated by (Heijnen et al., 1992a) and further generalized by (Kleerebezem and Loosdrecht, 2010), was used to estimate theoretical biomass yields for the different reaction steps involved in SO-NR, based on sulphide and elemental sulphur as electron donor and nitrate/nitrite as electron acceptor. Catabolic stoichiometry was solved for all the intermediate steps involved in SO-NR: both oxidation and reduction reactions were simplified in a 2-step reaction and no other intermediary products were considered except sulphur and nitrite, respectively. According to (Heijnen et al., 1992a), energy dissipation (ΔG_{dis}) in autotrophic metabolism appears strongly dependent on the fact that bacteria utilizes or not the reverse electron transport (RET) mechanism. Chemolithotrophic SOB are reported to adopt RET for C fixation but defining if and how efficiently bacteria adopt RET is not always straightforward since many metabolic mechanisms remain unclear (Klatt and Polerecky, 2015; Lin et al., 2018; Madigan et al., 2019; Yavuz et al., 2007) have applied the free Gibbs energy method to estimate the theoretical biomass yield of SOB, under the assumption that a highly energy-requiring RET mechanism was required for biomass synthesis, assuming $\Delta G_{dis} = 3500$ kJ/C-mol. Results from (Yavuz et al., 2007) have been used by (Can-dogan et al., 2010; Mora et al., 2015a) to support their experimental results. On the other hand, (Kleerebezem and Mendez, 2002) have compared the biomass yield obtained in their SOB-based work with values reported in literature. A total of 8 studies were reviewed, adopting mainly thiosulphate as electron donor but also sulphide and elemental sulphur; literature biomass yields were then used to derive overall metabolic energy dissipation, by applying the free Gibbs energy method in a bottom-up approach, and energy dissipation was estimated to be around 1500 ± 600 kJ/C-mol. Even though the standard deviation was as high as the 40%, the confidential interval falls below the value of 3500 kJ/C-mol, suggesting a more efficient energy uptake.

In the present work, full stoichiometry has been solved for all the possible reaction steps occurring in SO-NR, under the following two scenarios:

Energy dissipation, EDiss

1. EDiss_1 ΔGdis = 3500 kJ/C-mol;
2. EDiss_2 ΔGdis = 1500 kJ/C-mol (average value from Kleerebezem and Mendez, 2002)

Another aspect discussed in this section is the biomass formulation used in the stoichiometries available in literature. Some studies report a C-mol formulation of CH1,8O0,5N0,2 as reported by Roels (1983); some others a 5C-mol formulation of C5H7O2N (Rittmann and McCarty, 2001). Normalizing the second formulation to one C-mol, biomass stoichiometry results in CH1,4O0,4N0,2, slightly different for H and O fractions. The presented methods and hypotheses have been applied to both of the biomass composition (BC): BC_1: CH1,8O0,5N0,2 (Roels, 1983) and BC_2: CH1,4O0,4N0,2 (normalized to 1 C-mol from Rittmann and McCarty, 2001).

As general assumptions, one single SO-NR biomass is assumed for all the possible reactions, CO2 (as $HCO3^-$) and $NH4^+$ are considered as C and N source, respectively. The derived theoretical biomass yield was conducted and compared with literature values.

2.3. Model selection

A bibliographical research was conducted in order to screen out the various approaches adopted in mathematical modeling of autotrophic denitrification rates, with the final aim of assessing their capability of simulating the experimental data on nitrite accumulation presented by (Polizzi et al., 2022).

In order to establish a common ground among the available publications, only the works matching the following criteria were considered: 1) processes were modelled through rate-limited reactions, i.e. no mass transport limitations; 2) SO-NR was modelled through the four main steps presented in equations (1)–(4), referred to as process 1, 2, 3 and 4, herein; 3) one single biomass was considered for all the reactions; 3) operational conditions were in the typical/optimal ranges of pH and temperature for autotrophic denitrification processes (7–8 and 22–30 °C, respectively, according to (Deng et al., 2021)). Five models were selected, and special attention was devoted to the kinetic functions and parameters regulating uptake rates among the different reactions, in each model structure. Specifically, the following aspects were analyzed:

- Substrate uptake kinetics: Monod-type *vs* Haldane-type;
- Half-saturation coefficients: same value assumed for a given substrate in all the processes *vs* different values depending on the process;
- Maximum growth rates: same value assumed for all the processes *vs* different values for each process.
- Switch functions for the competition among electron acceptors/donors: adopted *vs* not adopted.

A summary of the main assumptions of the selected mathematical models is shown in Table 1; complete growth rate formulations of each model is reported in Table S5 of the supplementary material.

Each model was solved using the Gear numerical method in Matlab R2020B software (toolbox ode15s). Experimental biomass yields available in (Polizzi et al., 2022) were used in all the models instead of the default values, with further assumptions derived in the thermodynamic study and described in section 3.1. Table S4 reports the stoichiometric matrix applied to all the models.

2.4. Model comparison procedure

The multi-step procedure shown in Fig. 1 and described in the next sections was implemented in order to evaluate models' suitability to represent the observed data.

- STEP 1. First, a sensitivity analysis was performed in order to assess the three most sensitive parameters of each model. The sensitivity analysis was a local analysis, i.e., the effect of each parameter over the simulated output variables was assessed varying each parameter by a 10% increase and decrease, one at a time. The analysis was performed three times for every model, one for each experimental phase (see Table S1), to reach steady-state simulated outputs. Thus, the relative sensitivity (S_{ij}) of a steady-state output θ_i with respect to a parameter γ_j was calculated according to Equation (5) (Reichert and Vanrolleghem, 2001):

$$S_{ij} = \frac{\theta_i}{\gamma_j} \frac{d\gamma_j}{d\theta_i} \quad \text{Eq. (5)}$$

The two output variables used for this analysis were nitrate NO_3^- (mgN/L) and nitrite NO_2^- (mgN/L). Due to the uncertainties on the experimental data on the sulphur species (see section 2.1), the latter were not included in the sensitivity analysis nor in the objective function of the calibration procedure, but rather used for a qualitative validation of the calibrated models. The average of both sensitivity absolute values (±10%) was first calculated for each parameter and output. Then, the average of the values obtained per each of the two output variables was

Table 1
Summary of the mathematical models considered in this study. Default stoichiometric parameters were not used in the present study, see section 2.3.

Model	No. of kinetic parameters		Substrate uptake kinetics		Substrate affinities among processes		Switch functions	No. of stoichiometric parameters	Experimental data
	Tot	μ_{max}	Monod	Haldane	Constant value	Non-constant value	Non-competitive inhibition		
(Xu et al., 2014)	18	4	S^0, NO_3^-, NO_2^- [a]	S^{2-}, NO_2^- [a]	–	S^{2-}, S^0, NO_3^-, NO_2^-	NO_3^- over NO_2^- NO_2^- over NO_3^- [b]	1	Batch tests with autotrophic and/or heterotrophic denitrification.
Mora et al. (2015a)	12	4	S^0, NO_3^-	S^{2-}, NO_2^-	S^{2-}, S^0, NO_3^-, NO_2^-	–	S^{2-} over S^0	1	Autotrophic denitrification in respirometric batch tests.
(Hauduc et al., 2019)	11	2 [c]	S^0, NO_3^-	S^{2-}, NO_2^-	S^{2-}, S^0	NO_3^-, NO_2^-	S^{2-} over S^0 [d]	1	Literature review.
(Xu et al., 2016)	5	1	S^{2-}, NO_3^-, NO_2^-	None	S^{2-}, S^0, NO_3^-, NO_2^-	–	–	4	Autotrophic denitrification in a sequential batch reactor
(Huo et al., 2022)	11	4	S^{2-}, S^0, NO_3^-, NO_2^-	None	S^{2-}, S^0	NO_3^-, NO_2^-	–	2	Autotrophic denitrification in batch tests from Cui. et al. (2019), and coupled autotrophic denitrification-Anammox in batch tests from Deng et al. (2021).

[a] The Monod term for nitrite is only present in process 4. The Haldane term for nitrite is only present in process 2. Both Haldane terms use different inhibition constants for processes 1 and 2, and 2 and 4, for $S^{2-}$and NO_2^-,respectively.
[b] The switch term accounting for outcompetition of nitrate over nitrite is only present in process 3. The switch term for outcompetition of nitrite over nitrate is only present in process 1.
[c] Each μ_{max} and biomass/substrate yield value for each electron donor – uptake processes ($S^{2-}$and S^0).
[d] The switch term accounting for outcompetition of sulphide over sulphur is only present in process 3.

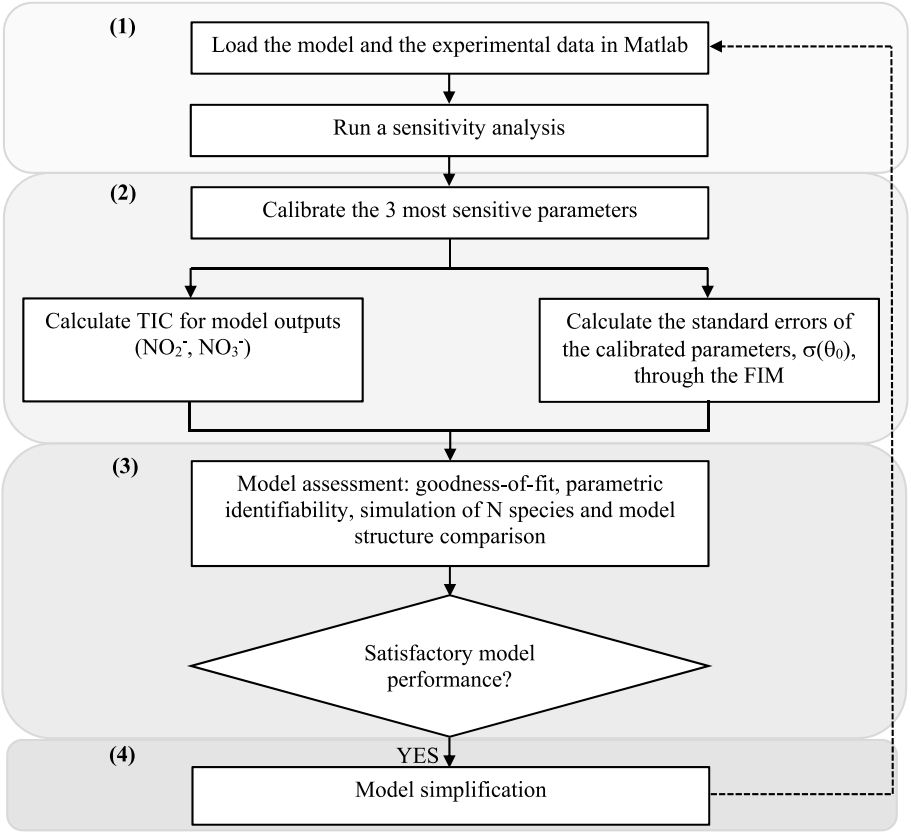

Fig. 1. Flow chart of the model comparison procedure. FIM refers to the Fisher Information Matrix while TIC refers to the Thiel Inequality Coefficient.

calculated to obtain a single sensitivity value for each parameter and phase. Therefore, in each case a *p x r* sensitivity matrix was obtained, where *p* is the number of parameters analyzed and *r* is the number of experimental phases considered.

- STEP 2. After performing the sensitivity analysis, the 3 most sensitive parameters (i.e., the parameters with the highest relative sensitivities) were selected for calibration. Parameter calibration was carried out by using the simplex search method of (Lagarias et al., 1998), which

is included in Matlab by using the toolbox *fminsearch*. The fitting of the experimental data considered NO_3^- (mgN/L) and NO_2^- (mgN/L) to minimize the objective function (F) (Eq. (6)). Function *F* was defined as the sum of the norm of the differences between model predictions and the experimental data for each output variable *y*:

$$F = \sqrt{\sum_{j=1}^{m}\sum_{i=1}^{n}\left[y_{exp,i} - y_{mod,i}\right]^2} \quad \text{Eq. (6)}$$

where m is the number of output variables, n is the number of experimental data, $y_{exp,i}$ is the experimental value and $y_{mod,i}$ is the predicted value. In order to avoid inconsistency of calibrated parameter values with empirical evidenced, the calibration was limited within an "consistency range", whose upper and lower values were set according to literature. The assumed range for each parameter can be found in the supplementary material (Table S8).

The fit of each calibrated model was quantitatively assessed through the Thiel Inequality Coefficient (TIC). This index is specifically appropriate to compare different models and was calculated according to Equation (7) (Huiliñir et al., 2010):

$$TIC = \frac{\sqrt{\sum_{i}^{m}\left(y_{exp,i} - y_{mod,i}\right)^2}}{\sqrt{\sum_{i}^{m} y_{exp,i}{}^2} + \sqrt{\sum_{i}^{m} y_{mod,i}{}^2}} \quad \text{Eq. (7)}$$

TIC values range between 0 and 1, being 0 a model output with no differences with the experimental data (i.e., a model with no errors in its predictions) and 1 the limit value when differences tend to be infinite. It is generally accepted to consider a maximum TIC of 0.3 as the threshold for a good fit of the modeling results (Hvala et al., 2005).

Model identifiability was evaluated through the FIM (Fisher Information Matrix) methodology (Guisasola et al., 2006) in order to calculate the confidence intervals of the calibrated parameters. The FIM is a *pxp* matrix, where *p* is the number of parameters, that incorporates the sensitivity functions of the calibrated parameters and the error of the experimental measurements. It is particularly useful to evaluate model structures and their capacity to reduce uncertainty in their predictive responses, since the presence of misspecifications in a given model (e.g., inclusion of extraneous variables or omission of relevant variables) might lead to incorrect parameter estimations (Guisasola et al., 2006a; Quaglio et al., 2018).

- STEP 3: The performance of the calibrated models was compared considering the goodness of fit of the modelled N species dynamics throughout the three experimental phases, in light of the results of step 2.
- STEP 4. After evaluating the best-fitting models for this study, one last effort was done in order to evaluate whether further structure simplification was possible without hampering the stability of the model output. To do that, the methodology of Fig. 1 was applied again to the new simplified model versions.

Moreover, beyond the analyzed models, an alternative 2-population modelling approach was investigated and results are presented in the supplementary material (see section S4). This parallel modelling effort falls out of the main scope of this study, but it is presented as an illustrative and complementary approach that can be applied to simulate the population shift observed in Polizzi et al., 2022).

3. Results and discussion

3.1. Thermodynamic theoretical framework: exploring the boundaries of SOB yield factor

Catabolic reactions for the possible intermediate steps in SO-NR process have been solved and results are presented in Table S2, whereas the full metabolic reactions are reported in tables S3a-b. Table 2 reports a synthesis of the biomass yields derived for each catabolic step, under the two assumptions on energy dissipation and biomass composition. Biomass yields (herein referred as Y) are reported both as C-mol/S-mol and C-mol/e-mol (i.e. C-mole production per electron mole released during the ED oxidation). At each ED oxidation reaction, biomass yield, either as C-mol/S-mol or C-mol/e-mol, varies by 27–29%, depending on the TEA reduction reaction that is used in catabolism. Such a wide range is to be ascribed to the fact that 2 to 5 electrons can be accepted in the TEA reduction steps, thereby affecting the free Gibbs energy available from catabolism and, ultimately, the λCat determining the full metabolism stoichiometry (Kleerebezem and Loosdrecht, 2010). The last three rows of Table 2 summarize the Y values for each ED oxidation step, reporting average value and standard deviation, calculated over the three possible TEA reduction cases. Considering biomass yields expressed as C-mol/S-mol, the values from the oxidation reaction $HS^- \rightarrow S^0$ is almost half of the one obtained from the reaction $S^0 \rightarrow SO4^{2-}$ and almost one third of the one from reaction $HS^- \rightarrow SO4^{2-}$, consistently with the fact that 2, 4 and 6 electrons are released in each reaction, respectively, as well as with previous results presented in the literature (Deng et al., 2021b; Mannucci et al., 2012a). Such an evidence is in line with the results of biomass yields normalized to the electron released at each corresponding ED oxidation step. All the yields as C-mol/e-mol, in fact, exhibit values of 0.23 and 0.47 C-mol/e-mol, for the assumption of 3500 and 1500 kJ/C-mol, respectively.

It can be easily observed that the hypothesis on the overall energy dissipation is much more relevant than the one on the biomass composition, resulting in 50% of variation, if the two values of 3500 or 1500 kJ/C-mol are considered. Indeed, only 1–2% variation is observed comparing the results from the two biomass compositions. In the biomass composition from (Savageau, 1984), CH1,8O0,5N0,2, the oxidation state of carbon is 0.2 and 4.2 e-mol/C-mol are required to the reduction of CO2 to biomass. In the biomass composition from Rittmann and McCarty (2001), CH1,4O0,4N0,2, the oxidation state of carbon is 0 and 4 e-mol/C-mol are required instead. Thereby, it is reasonable that such a minor difference in electron requirement (0.2 e-mol/C-mol) implies a comparable requirement of electron donor in anabolism.

Biomass yields available in literature have been evaluated and gathered according to the corresponding catabolic reaction considered in each work. Only works where sulphide or sulphur were used as electron donor were considered and results are summarized in Table 3. Nevertheless, the values reported by (Kleerebezem and Mendez, 2002) are considered as representative also of the experimental values using thiosulphate as electron donor, since the literature review presented by the authors encompasses works based on thiosulphate, sulphur and sulphide oxidation (coupled with denitrification) and anaerobic cellular yields on sulphide consumption are reported to be comparable with that on thiosulphate for *T. denitrificans* (Hoor and Cell, 1981). When the information reported was sufficient, biomass yield unit conversion has been calculated for each study. Note that the use of granular or biofilm-based biomass in UASB-like reactors are often reported, but biomass concentration is rarely assessed. Thereby, many studies on denitrifying SOB could not be used in this literature review due to the lack of information on biomass growth.

As presented in Tables 2 and 3, the biomass yields observed by (Polizzi et al., 2022) is among the lowest reported in literature. The theoretical yields derived under the two assumptions of energy dissipation, at all the SO-NR catabolic steps, are reported in tables S3a-b; it can be observed that the experimental yield of the reference study is close to the values obtained with the assumption of high energy dissipation. To the best of our knowledge, no other works report on biomass yields in process operating mainly (or exclusively) the denitratation step. (Klatt and Polerecky, 2015) report a study on SOB proposing a new theoretical approach to estimate microbial bioenergetics efficiency, based on the factorization of the metabolic aspects involved in energy

Table 2
Main results from biomass yield study.

	ΔG^{01}_met = 3500 kJ/Cmol				ΔG^{01}_met = 1500 kJ/Cmol			
	C-mol_biom/S-mol		C-mol_biom/e-mol		C-mol_biom/S-mol		C-mol_biom/e-mol	
	$CH_{1,8}O_{0,5}N_{0,2}$	$CH_{1,4}O_{0,4}N_{0,2}$	$CH_{1,8}O_{0,5}N_{0,2}$	$CH_{1,4}O_{0,4}N_{0,2}$	$CH_{1,8}O_{0,5}N_{0,2}$	$CH_{1,4}O_{0,4}N_{0,2}$	$CH_{1,8}O_{0,5}N_{0,2}$	$CH_{1,4}O_{0,4}N_{0,2}$
$HS^- \rightarrow SO_4^{2-}$ $NO_3^- \rightarrow N_2$	0.189	0.191	0.024	0.024	0.383	0.392	0.048	0.049
$HS^- \rightarrow SO_4^{2-}$ $NO_2^- \rightarrow N_2$	0.228	0.231	0.028	0.029	0.452	0.463	0.056	0.058
$HS^- \rightarrow SO_4^{2-}$ $NO_3^- \rightarrow NO_2^-$	0,126	0,128	0,016	0,016	0.266	0.272	0.033	0.034
$HS^- \rightarrow S^0$ $NO_3^- \rightarrow N_2$	0.050	0.050	0.025	0.025	0.101	0.103	0.050	0.052
$HS^- \rightarrow S^0$ $NO_2^- \rightarrow N_2$	0.060	0.060	0.030	0.030	0.118	0.121	0.059	0.060
$HS^- \rightarrow S^0$ $NO_3^- \rightarrow NO_2^-$	0.034	0.035	0.017	0.017	0.072	0.074	0.036	0.037
$S^0 \rightarrow SO_4^{2-}$ $NO_3^- \rightarrow N_2$	0.139	0.141	0.023	0.023	0.282	0.289	0.047	0.048
$S^0 \rightarrow SO_4^{2-}$ $NO_2^- \rightarrow N_2$	0.168	0.171	0.028	0.028	0.334	0.342	0.056	0.057
$S^0 \rightarrow SO_4^{2-}$ $NO_3^- \rightarrow NO_2^-$	0.092	0.093	0.015	0.015	0.194	0.198	0.032	0.033
$HS^- \rightarrow SO_4^{2-}$	0.181	0.183	0.023	0.023	0.367	0.376	0.046	0.047
$HS^- \rightarrow S^0$	0.048	0.048	0.024	0.024	0.097	0.099	0.049	0.050
$S^0 \rightarrow SO_4^{-}$	0.133	0.135	0.022	0.022	0.270	0.276	0.045	0.046
$HS^- \rightarrow SO_4^{2-}$	**0.18 ± 0.05**		**0.023 ± 0.006**		**0.37 ± 0.09**		**0.046 ± 0.012**	
$HS^- \rightarrow S$	**0.05 ± 0.01**		**0.024 ± 0.006**		**0.10 ± 0.02**		**0.049 ± 0.012**	
$S \rightarrow SO_4^{2-}$	**0.13 ± 0.04**		**0.022 ± 0.006**		**0.27 ± 0.07**		**0.046 ± 0.012**	

Table 3
Literature and theoretical values for SOB yield factor.

	Y				Reference	Method
	1C-mol/S-mol	1C-mol/e-mol	g_biom/gS	g_biom/gN		
$HS^- \rightarrow SO_4^{2-}$	0.512	0.064	0.378	0.635	(Sublette and Sylvester, 1987)	Experimental
$NO_3^- \rightarrow N_2$	0.333	0.042	0.256	0.451	Kleerebezem and Mendez, 2002	Review/Thermodynamics calculations
	0.511	0.064	0.361	0.694	Campos et al. (2008)	–
	0.184	0.023	0.130	0.208	Can-Dogan et al. (2010)	Thermodynamic calculations[b] confirmed by experimental evidence
	0.465	0.058	0.328	0.610	Mora et al., 2014	Experimental
	0.156	0.019	0.118	0.149	Polizzi et al., 2022[a]	Experimental
	0.189–0.383	0.023–.046	0.145–0.294	0.230–0.526	This study[c]	Thermodynamic calculations
$HS^- \rightarrow S^0$	0.159	0.08	0.562		(Gadekar et al., 2006)	Experimental and modelling
$NO_3^- \rightarrow N_2$	0.046	0.023	0.032		Can-Dogan et al. (2010)	Thermodynamic calculations[b] confirmed by experimental evidence
			0.13–0.37		Xu et al., 2016	Experimental and modelling
	0.065	0.033	0.046	0.300	Mora et al., 2014c	Experimental
	0.050–0.1	0.025–0.05	0.038–0.077	0.244–0.563	This study[c]	Thermodynamic calculations
$S^0 \rightarrow SO_4^{2-}$	0.364	0.061	0.257	0.646	(Sahinkaya et al., 2011)	–
$NO_3^- \rightarrow N_2$	0.400	0.067	0.283	0.737	Mora et al., 2014c	Experimental
	0.364	0.061	0.257	0.646	(Batchelor and Alonzo, 1978)	Experimental
			0.21–0.38		Xu et al., 2014	Calibration on continuous experiment modelling

[a] Estimated in a system performing PAD as the main reaction.
[b] Free Gibbs energy method, under the hypothesis of ΔG_{DISS} of 3500 kJ/C-mol.
[c] Theoretical yield according to the free Gibbs energy change method, under the hypothesis of ΔG_{DISS} of 3500 kJ/C-mol (lower limit) and 1500 kJ/C-mol (upper limit).

conversion and production. Specifically, for SOB bacteria, the energetic efficiency of the following aspects is considered: (i) energy production in the catabolic reaction, depending on the Sulphur metabolic pathway used by the microorganism; (ii) CO_2 fixation cycles and (iii) electron donor consumption in RET for the reducing power to be produced (NAD(P)H, $FADH_2$ or reduced Ferredoxin). Even though, such a new method is not implemented in the present study, it is of interest to highlight the underlying assumptions and conclusions proposed by the authors, since they clarify how the actual microbial bioenergetics also depends on the specific bacteria involved and the metabolic pathways adopted. It is remarkable to highlight that, in the reference study, energy optimization mechanisms are speculated to have promoted the population shift observed in the reference work, where energy-limiting conditions were determined by steady electron donor limitation. In line with such a consideration is the observed outcompetition of the more energy-efficient *Thiobacillus* genus over the *Sulphurimnas* genus (Klatt and Polerecky, 2015; Polizzi et al., 2022).

3.2. Model implementation, sensitivity analysis and calibration results

According to the study on the electron availability in the first and second step of HS^- oxidation, the experimental biomass yield of 0.117 g_biom/gS, observed over the complete HS^- oxidation to SO_4^{-}, was proportionally recalculated for each oxidation step; such an approach is

in line with yields reported in other works (Deng et al., 2021; Mannucci et al., 2012). The yields resulted in 0.029 g_biom/gS, for process 1 and 3, and 0.088 g_biom/gS, for process 2 and 4, and were adopted in each of the five model instead of their default value.

3.2.1. Sensitivity analysis

The results of the sensitivity analysis for each model are shown in Table S7. The parameters that showed higher sensitivities are directly involved in nitrate and nitrite reduction: maximum specific growth rates (μ_{max}), semisaturation coefficients (ks_{NO3} and ks_{NO2}) and inhibition constants (ki_{NO2} and k_{switch}). In the simulations related to the sensitivity analysis, simulated sulphide and elemental sulphur were barely observable throughout phases 1b and 2 (data not shown); thereby, semi-saturation coefficients and inhibition constants referring to sulphide and sulphur did not show any significant impact. Nevertheless, in phase 3 a general increase of parameter sensitivity was observed. According to (Polizzi et al., 2022), S^0 accumulation probably occurred at this last phase and was likely related to the higher and less stable influent S/N, compared to the other phases. Consistently, the sensitivity of the parameters involved in processes 3 and 4, such as semi-saturation coefficients for S^0, is higher in the 3rd phase (see Table S7).

Noticeably some models showed, on average, higher sensitivity in their parameters than others. For instance (Hauduc et al., 2019), was the least sensitive model to its kinetic parameters, as a general behaviour. When looking at the default performance of this model, it was noticeable how steady-state values for nitrite were approaching a value of 0 under all three experimental phases. As a consequence of such limitation, most parameters did not show any significant effect over the simulated values; in fact, only 1 parameter displayed a sensitivity higher than 0.25 in any of the 3 phases – which is considered the threshold for significant influence of a parameter over a variable (Cao et al., 2021). On the other hand (Xu et al., 2016), showed very high sensitivity (>3, on average) to its kinetic parameters and (Mora et al., 2015a) had a total of 9 parameters with values higher than the 0.25 threshold in, at least, one phase, which suggested that the model was more sensitive to its parameters under the applied conditions.

3.2.2. Parameter calibration and identifiability

Dynamic calibration comprised the optimization of the three most relevant parameters of each model, using the experimental dataset from the full-operation of the reference study. Parameters' calibrated values are shown in Table 4 along with their confidence regions calculated with the FIM. Results on the objective function and the TIC criteria are also provided in Table 4.

As presented in Table 4, the goodness-of-fit among the different models was quite different as suggested by the wide range of the F values, from a value of 230–621. TIC_{NO2} and TIC_{NO3} are also a measure of how well the simulated data fits with the experimental dataset for nitrite and nitrate, respectively. Consistently, as shown in Table 4, the higher the F value of a given model, the higher the TIC values. The highest F and TIC values are observed by the models from (Hauduc et al., 2019; Xu et al., 2016), both showing TIC_{NO2} above the critical threshold. On the contrary, the lowest F and TIC values are observed for the models from (Mora et al., 2015a; Huo et al., 2022). In terms of F and TIC values, the model proposed by (Xu et al., 2014) showed intermediate values compared to the above-mentioned models, with the TIC_{NO3} slightly below the critical threshold. Also noteworthy, optimized parameters with extreme values close to the limits set during calibration were obtained in those models where the goodness-of-fit was not satisfying (see Table S6), i.e., models by (Xu et al., 2016; Hauduc et al., 2019; Xu et al., 2014). Regarding parameter identifiability, the models from (Mora et al., 2015a; Huo et al., 2022) showed the narrower range for the confidence interval for the three optimized parameters.

3.2.3. Model assessment: analysis of fit, parameter identifiability and process rates

Fig. 2 shows the N species profiles of each model, after calibration. A discussion on the outcomes on parameters' calibration, goodness-of-fit and parametric identifiability is presented as a baseline for models' comparison.

Results on models' accuracy were in agreement with the outcomes described in the previous section. Indeed, the calibrated models from (Xu et al., 2014; Mora et al., 2015a; Huo et al., 2022) were generally capable to represent NO_2^- accumulation with good accuracy under the three experimental conditions (TIC_{NO2} >0.14 all three models). On the contrary, the calibrated models from (Hauduc et al., 2019)) and of (Xu et al., 2016)) resulted in poorer fits for NO_2^- (TIC_{NO2} = 0.32 and TIC_{NO2} = 0.49, respectively), in all the three phases. Remarkably, all models showed a good representation of the volatile suspended solids (VSS) dynamics (see Fig. S2), which demonstrated the adequacy of the experimental biomass/substrate yields from (Polizzi et al., 2022). Also sulphate and elemental sulphur concentrations were in line with the experimental data (see Figs. S2 and S3). Specifically, elemental sulphur accumulation during phase 3 was predicted by the five models, in accordance with the experimental findings by (Polizzi et al., 2022).

An in-depth analysis of the biomass growth rates, in process 1 to 4, has been conducted in order to better discern the reasons underlaying models' outcomes discrepancies. Fig. 3 reports the average biomass growth rates from the 5 calibrated models, for processes 1 to 4, at each operational phase (Hauduc et al., 2019; Xu et al., 2016). showed high rates in the reduction step $NO_2^- \rightarrow N_2$ (involved in processes 2 and 4), which appeared to limit NO_2^- accumulation; the rate of process 4 was, on average, 4.6 and 6 times higher in (Hauduc et al., 2019; Xu et al., 2016), respectively, compared to the other three calibrated models. Process 4

Table 4
Models' calibration outcomes: Optimum parameters' value and their confidence regions, calculated with the FIM and presented in parenthesis, as absolute and relative value (%); objective functions values and the TIC values for NO_2^- and NO_3^- fits.

Model	Optimized parameters			F value	TIC_{NO2}	TIC_{NO3}
(Xu et al., 2014)	$\mu_{max,1}$ = 7.68 d^{-1} (±11.08) (±144.35%)	$\mu_{max,3}$ = 0.72 d^{-1} (±0.002) (±0.3%)	$k_{switch,\ NO2}$ = 190.41 mgN/L (±682.50) (±358.44%)	314	0.13	0.27
Mora et al. (2015a)	$\mu_{max,3}$ = 2.17 d^{-1} (±0.01) (±0.67%)	$\mu_{max,4}$ = 0.67 d^{-1} (±0.06) (±9.58%)	ki_{NO2} = 102.43 mgN/L (±1.53) (±1.49%)	225	0.10	0.18
(Hauduc et al., 2019)	$\mu_{max,2}$ = 1.64 d^{-1} (±0.003) (±0.19%)	$ks_{NO2,\ S0}$ = 110.00 mgN/L (±8.25) (±7.51%)	$ks_{NO2,\ HS}$ = 110.00 mgN/L (±41.38) (±37.61%)	458	0.32	0.16
(Xu et al., 2016)	ks_{NO2} = 109.93 mgN/L (±1.29) (±1.2%)	$\mu_{max,1}$ = 6.78 d^{-1} (±9.77) (±144.1%)	nS = 0.176 (±10.03) (±5700%)	621	0.49	0.31
(Huo et al., 2022)	Ks_{S0} = 3.68 mgS/L (±0.64) (±17.46%)	$\mu_{max,3}$ = 1.58 d^{-1} (±0.03) (±2.30%)	$\mu_{max,4}$ = 0.09 d^{-1} (±0.003) (±3.70%)	230	0.11	0.20

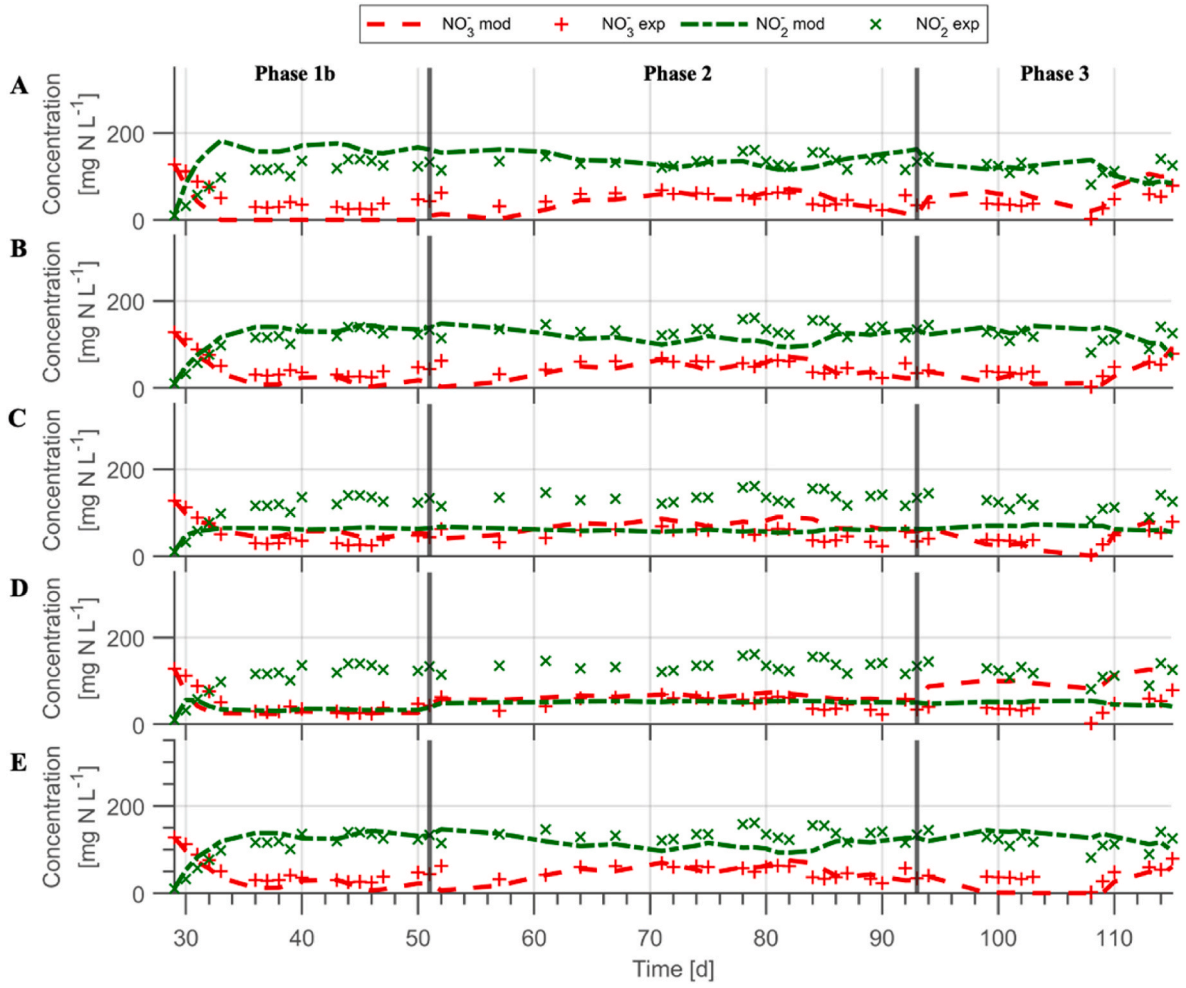

Fig. 2. Data fitting of the calibrated models on nitrate and nitrite: A) (Xu et al., 2014), B) (Mora et al., 2015a), C) (Hauduc et al., 2019), D) (Xu et al., 2016), E) (Huo et al., 2022). Vertical lines in bold delineate the three experimental phases (1, 2 and 3).

was, overall, much slower than process 3 in all models that could effectively predict nitrite accumulation. This suggests a better capacity of nitrate to oxidize S^0, which is in line with the findings of (Cai et al., 2022; Li et al., 2021). In (Xu et al., 2016), the source of this limitation comes from the calibrated maximum specific growth rate (one single value, according to model structure), whose value was as high as $\mu_{max,1} = 6.78\ d^{-1}$ (2.26 and 6 times higher than the average calibrated values for processes 2 and 4, respectively, see Table S6). The optimization procedure was likely constrained by a deficient capacity of the model to simulate NO_3^- reduction, as a consequence of the low affinity for nitrite reported in that study ($ks_{NO3} = 109$ mgN/L, 2–3 orders of magnitude higher than the average reported values, see Table S6). It is worth mentioning that the uncertainty analysis performed in (Xu et al., 2016) revealed large confidence intervals (±95%) for the paired set of parameters ks_{NO2}-ks_{NO3} and ks_{NO3}-ks_{HS}.

In the case of (Hauduc et al., 2019), the high affinity for S^0 and the lack of a non-competitive terms for HS- over S^0 resulted in a high rate of process 4 throughout all phases, as it can be observed in Fig. 3. As a result, the calibration phase in both models led to high values for the optimized values for ks_{NO2}: 1–3 orders of magnitude higher than the average literature values (approaching the upper limit of 110 mgN/L).

The model from (Xu et al., 2014) properly fits experimental data in phases 2 and 3, whereas in phase 1 all NO_3^- was reduced to NO_2^-, i.e., no NO_3^- was observed as shown in Fig. 2. The reason of that comes from the calibrated $\mu_{max,1}$, with an optimized value 3 times higher than the average reported values (see Table S6), over-enhancing process 1 as a result; in this model, the rate of process 1 was 29% higher than the other models (see Fig. 3). Also, low NO_2^- reduction rates led to its excessive accumulation in phase 1 (see Fig. 2). Furthermore, the wide confidence intervals for two out of three of the optimized parameters indicated a very high uncertainty of the calibrated parameters (Table 4). The cause of this misestimation was attributed to the different kinetic terms and parameters of the model. For instance, substrate inhibitions play a different role in the different processes: in the case of nitrite inhibition, a Haldane term is present in the growth rate formulation of process 2 but not in process 4, whereas in the case of sulphide inhibition, it is considerably stronger in process 2 than in process 1 ($k_{i,\ HS,1} = 2053.2$ $mgSL^{-1}$ and $k_{i,\ HS,2} = 1.38$ $mgSL^{-1}$, see Table S6). Therefore, process 2 was completely hindered (as can be seen in Fig. 3), consequently affecting the calibration outcomes. Nevertheless, the model was able to predict NO_2^- accumulation under the experimental conditions of phases 2 and 3, as confirmed by low values of TIC_{NO2} and TIC_{NO3}.

Both models from (Mora et al., 2015a; Huo et al., 2022) properly fit nitrate and nitrite profiles in the three experimental conditions, and the resulting confidence intervals of the estimated parameters were significantly lower than in the other models (see Table 4). (Mora et al., 2015a) confidence intervals were all below ±10% while in (Huo et al., 2022), the confidence region for Ks_{S0} was ±17.5%, which suggests a slightly worse parametric identifiability. The latter might be a consequence of two peculiarities of the model structure: (1) no inhibition is represented for any substrate, unlike (Mora et al., 2015a) where Haldane inhibitions are formulated for nitrite and sulphide; (2) the semi-saturation

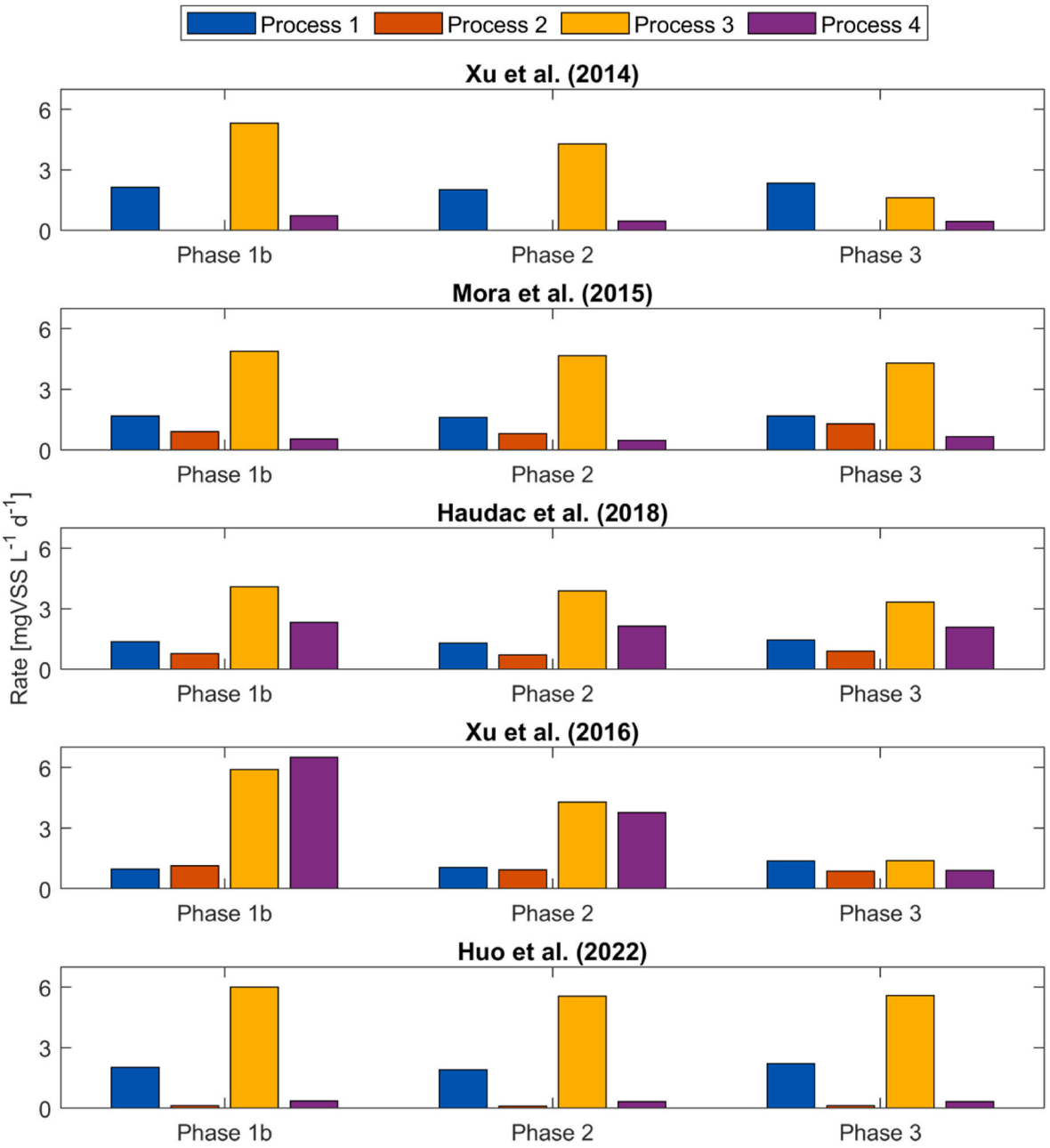

Fig. 3. Average biomass growth rates for the different SO-NR processes (1–4), for each model and experimental phase.

coefficients for N species were not sensitive because their default values are very low – between 0.1 and 0.21 mgN/L (Table S6) – and the varying affinities among processes are not relevant when using the model under this specific experimental dataset, where the concentration of both NO_3^- and NO_2^- in the system are far above the semi-saturation coefficients. As a result, the model is highly dependent on a limited set of parameters, mainly the maximum specific growth rates (see Table S7), and it is not as identifiable as (Mora et al., 2015a). The importance of calibrating parameters in high-sensitivity regions is highlighted by the fact that, among the optimized parameters of these two models, the ones that were less sensitive in phase 3 were also less identifiable (higher confidence regions). Therefore, a different selection procedure for parameter calibration with a stronger focus on phase 3 could have possibly improved both the goodness-of-fit and the parametric estimations.

In light of the presented model-specific discussion (Mora et al., 2015a), is suggested as the most suitable model structure to describe nitrite accumulation observed in (Polizzi et al., 2022). Specifically, this model achieved the best fit with the experimental data, along with (Huo et al., 2022); the goodness-of-fit was very similar in both models according to the obtained TIC values for NO_3^- and NO_2^-, but it is considered that the model from (Mora et al., 2015a) holds a more rigorous structure since it accounts for substrates' inhibition and uptake competition, widely observed and reported in literature. Indeed, both nitrite and sulphide have been described as an inhibitor for denitrifying SOB cultures at different concentration ranges (Mora et al., 2015b). reported nitrite inhibition concentrations as low as 11.5 mgN/L in a non-acclimated culture, and as high as 75.4 mgN/L in previously-acclimated to nitrite biomass (Wang et al., 2022; Cai et al., 2022). found nitrite to be inhibiting between 36 and 60 mgN/L (Fajardo et al., 2014), reported a Haldane nitrite inhibition constant of 34.7 mgN/L and (Claus and Kutzner, 1985) observed nitrite inhibition at concentrations over 200 mgN/L. The calibrated inhibition constant for nitrite obtained in this work was $ki_{NO2} = 102.43$ mgN/L, which is about 50% higher than the values generally reported in the literature. Possibly,

biomass acclimation to the substrate hindered the inhibitory effect of nitrite. Moreover, the use of slightly basic conditions in the experimental setup (pH = 7.6) could have led to lower concentrations of free nitrous acid (FNA), generally accepted as the actual inhibitory form of nitrite (Zhou et al., 2011). High concentrations of sulphide – over 80 mgS/L – have also been reported to be inhibitory on autotrophic denitrification by many authors (Lan et al., 2019; An et al., 2010; Li et al., 2021; Lu et al., 2018; Fajardo et al., 2014); even though this Haldane term has little relevance in this specific case, since there is no sulphide accumulation, its inclusion is deemed relevant to simulate other experimental studies with a higher sulphide loading rate and/or S/N ratio.

In conclusion, including substrate inhibition is considered a plus for the accuracy of the model, but the experimental data could be properly represented by means of standard Monod terms in the growth rate expressions, as demonstrated by the calibration results of (Huo et al., 2022).

3.2.4. Exploring possible model simplifications

An effort to simplify the ultimately selected model was performed. A sensitivity analysis and calibration procedure were again performed on (Mora et al., 2015; Huo et al., 2022). The following modification to the models were arbitrarily selected and implemented: the four μ_{max} were grouped into two μ_{max}; one for processes 1 and 2, and another one for processes 3 and 4, using the default $\mu_{max,1}$ and $\mu_{max,3}$, respectively. The results of this approach are shown in Table S9, and the obtained representation of NO_2^-, and NO_3^- by the calibrated modified models is shown in Fig. S1.

Results show that (Mora et al., 2015), even with less parameters, could still represent the experimental data with good accuracy according to the resulting TIC for nitrite and nitrate, as well as the objective function. On the contrary, the modified version of (Huo et al., 2022) could not withstand the model simplification, and was not able to simulate experimental data properly, as can be observed in Fig. 4. Indeed, according to the sensitivity analysis (Table S7), the non-modified model from (Huo et al., 2022) relied strongly on $\mu_{max,3}$ and $\mu_{max,4}$ and the applied modifications strongly hampered its ability to represent nitrite accumulation. Moreover, the confidence regions obtained indicated a huge difference regarding parametric identifiability between the two models. Optimized parameters from (Huo et al., 2022) could not be accurately estimated because the model was remarkably depending on having 4 different μ_{max} values in order to simulate this data, whereas (Mora et al., 2015) was still identifiable. This evidence further indicates that a more complete and robust structure in the latter made it more adequate to simulate the observed nitrite accumulation. Results obtained also demonstrate the feasibility of developing simpler models to describe the PAD process.

4. Conclusions

This work provides a theoretical framework on the biomass yields as well as a comprehensive study comparing and analysing available kinetic models of SO-NR systems, with a specific focus on partial autotrophic denitrification supported by experimental evidences.

The theoretical framework on the biomass yield confirms that experimental values should be critically considered together with the specific conditions of the studied systems, due to the high variety of the involved SOB population and the strong influence of the operational conditions. Specifically, the low biomass yield estimated in the reference study on PAD is in line with the lower energy delivered in the catabolic reaction of partial nitrate reduction to nitrite (denitratation), and the comparison with theoretical values suggests that a high energy dissipation was involved. Moreover, it is speculated that energy constraints and energy optimization mechanisms are possibly behind the clear population shift observed.

The critical application, calibration and comparison of 5 published models showed that PAD dynamics can be successfully described through different modelling approaches. Sensitivity analysis of the selected models showed specific growth rates to be crucial parameters, especially under S/N ratios close to 1 gS/gN. Nitrite accumulation could be accurately predicted either by Haldane-type and Monod-type kinetics for its uptake in biomass growth rates. Nevertheless, a more thorough analysis on models' performance and parameters' identifiability revealed that the model including non-competitive inhibition for nitrite uptake, i.e., Haldane saturation function, showed higher accuracy and identifiability. Furthermore, the latter approach was found to be consistent enough to withstand model simplification, remaining able to represent the experimental dataset preserving parametric identifiability.

The reported results are considered a relevant contribution on the stoichiometry and kinetics governing the PAD process, especially in the perspective of process upscale and control. A better understanding of the PAD process, encompassing process bioenergetics and kinetics, allows to move step forwards its implementation in synergy with other innovative processes such as anammox or biogas biological removal of sulphide in innovative anoxic bioscrubbers.

Authors' contributions

E. Valdes: modelling work, writing, discussion. D. Gabriel: supervision, discussion and conceptualization, fund acquisition. D. Gonzalez: supervision, discussion. G. Munz: supervision, discussion and conceptualization, fund acquisition. C. Polizzi thermodynamic analysis, writing, supervision, discussion and conceptualization.

All the authors contributed to the revision of the work and agreed with the final version of the article.

Declaration of competing interest

The authors declare that there is no competing interest to disclose.

Data availability

Data will be made available on request.

Acknowledgements

This project has received funding from the European Union's Horizon 2020 research and innovation programme under the Marie Skłodowska-Curie grant agreement No 872053.

Appendix A. Supplementary data

Supplementary data to this article can be found online at https://doi.org/10.1016/j.chemosphere.2023.139605.

References

An, S., Tang, K., Nemati, M., 2010. Simultaneous biodesulphurization and denitrification using an oil reservoir microbial culture: effects of sulphide loading rate and sulphide to nitrate loading ratio. Water Res. 44, 1531–1541. https://doi.org/10.1016/j.watres.2009.10.037.

Baspinar, A.B., Turker, M., Hocalar, A., Ozturk, I., 2011. Biogas desulphurization at technical scale by lithotrophic denitrification: integration of sulphide and nitrogen removal. Process Biochem. 46, 916–922. https://doi.org/10.1016/j.procbio.2011.01.001.

Batchelor, Bill, Alonzo, W Lawrence, 1978. Autotrophic Denitrification Using Elemental Sulfur. Water Pollution Control Federation (50 (8):), 1986–2001.

Cai, J., Sun, Y., Qaisar, M., Wang, K., Chen, B., 2022. Revealing the effect of multiple nitrogen sources on sulfide oxidation by progressively changing nitrate to nitrite. Sep. Purif. Technol. 283 https://doi.org/10.1016/j.seppur.2021.120226.

Campos, J.L., Carvalho, S., Portela, R., Me, R., 2008. Kinetics of Denitrification using Sulphur Compounds: Effects of S/N Ratio, Endogenous and Exogenous Compounds, 99, pp. 1293–1299. https://doi.org/10.1016/j.biortech.2007.02.007.

Can-dogan, E., Turker, M., Dagasan, L., Arslan, A., 2010. Sulfide removal from industrial wastewaters by lithotrophic denitrification using nitrate as an electron acceptor. Water Resour. Ind. 2286–2293. https://doi.org/10.2166/wst.2010.545.

Chen, F., Li, X., Gu, C., Huang, Y., Yuan, Y., 2018. Selectivity control of nitrite and nitrate with the reaction of S0 and achieved nitrite accumulation in the sulfur autotrophic

denitrification process. Bioresour. Technol. 266, 211–219. https://doi.org/10.1016/j.biortech.2018.06.062.
Chen, F., Li, X., Yuan, Y., Huang, Y., 2019. An efficient way to enhance the total nitrogen removal efficiency of the Anammox process by S0-based short-cut autotrophic denitrification. J. Environ. Sci. 81, 214–224. https://doi.org/10.1016/j.jes.2019.01.010.
Claus, G., Kutzner, H., 1985. Physiology and kinetics of autotrophic denitrification by Thiobacillus denitrificans. Appl. Microbiol. Biotechnol. 22 https://doi.org/10.1007/BF00252031.
Cui, Y., Guo, G., Ekama, G.A., Deng, Y., Chui, H., Chen, G., Wu, D., 2019. Elucidating the Bio Fi Lm Properties and Biokinetics of a Sulfur-Oxidizing Moving-Bed Bio Fi Lm for Mainstream Nitrogen Removal 162, pp. 246–257. https://doi.org/10.1016/j.watres.2019.02.061.
Deng, Y., Tang, W., Huang, H., Qian, J., Wu, D., 2021. Development of a Kinetic Model to Evaluate Thiosulfate-Driven Denitrification and Anammox (TDDA) Process 198. https://doi.org/10.1016/j.watres.2021.117155.
Deng, Y.-F., Zan, F., Huang, H., Wu, D., Tang, W., Chen, G.-H., 2022. Coupling sulfur-based denitrification with anammox for effective and stable nitrogen removal: a review. Water Res. 224, 119051 https://doi.org/10.1016/j.watres.2022.119051.
Fajardo, C., Mora, M., Fernández, I., Mosquera-Corral, A., Campos, J.L., Méndez, R., 2014. Cross effect of temperature, pH and free ammonia on autotrophic denitrification process with sulphide as electron donor. Chemosphere 97, 10–15. https://doi.org/10.1016/j.chemosphere.2013.10.028.
Gadekar, S, Nemati, M Ã, Hill, G A, 2006. Batch and continuous biooxidation of sulphide by Thiomicrospira Sp . CVO : reaction kinetics and stoichiometry. Water Res. 40, 2436–2446. https://doi.org/10.1016/j.watres.2006.04.007.
Guisasola, A., Baeza, J.A., Carrera, J., Sin, G., Vanrolleghem, P.A., Lafuente, J., Matrix, F. I., 2006. The influence of experimental data quality and quantity on parameter estimation accuracy Andrews inhibition model as a case study. Educ. Chem. Eng. 1, 139–145.
Guo, Q., Hu, H.Y., Shi, Z.J., Yang, C.C., Li, P., Huang, M., Ni, W.M., Shi, M.L., Jin, R.C., 2016. Towards simultaneously removing nitrogen and sulfur by a novel process: anammox and autotrophic desulfurization-denitrification (AADD). Chem. Eng. J. 297, 207–216. https://doi.org/10.1016/j.cej.2016.03.138.
Hauduc, H., Wadhawan, T., Bruce, J., Bott, C., Ward, M., Takács, I., 2019a. Incorporating sulfur reactions and interactions with iron and phosphorus into a general plant-wide model Hélène Hauduc , Tanush Wadhawan , Bruce Johnson , Charles Bott. Water Sci. Technol. 79 (1), 26–34. https://doi.org/10.2166/wst.2018.482.
Heijnen, J.J., Loosdrecht, M.C.M., Tijhuis, L., 1992a. A black box mathematical model to calculate auto- and heterot rophic biomass yields based on Gibbs energy dissipation. Biotechnol. Bioeng. 40, 1139–1154.
Hoor, T., Cell, A., 1981. c o m p a r e d w i t h Thiobacillus denitrificans Netherlands. Institute for Sea Research , Texel. The Netherlands ' 47.
Huiliñir, C., Romero, R., Muñoz, C., Bornhardt, C., Roeckel, M., Antileo, C., 2010. Dynamic modeling of partial nitrification in a rotating disk biofilm reactor: calibration, validation and simulation. Biochem. Eng. J. 52, 7–18. https://doi.org/10.1016/j.bej.2010.06.012.
Huo, P., Chen, X., Yang, L., Wei, W., Ni, B., 2022a. Modeling of sulfur-driven autotrophic denitrification coupled with Anammox process. Bioresour. Technol. 349, 126887 https://doi.org/10.1016/j.biortech.2022.126887.
Hvala, N., Strmcnik, S., Sel, D., Milanic, S., Banko, B., 2005. Influence of model validation on proper selection of process models — an industrial case study. Comput. Chem. Eng. 29, 1507–1522. https://doi.org/10.1016/j.compchemeng.2004.11.013.
Klatt, Judith M., Polerecky, L., 2015. Assessment of the stoichiometry and efficiency of CO 2 fixation coupled to reduced sulfur oxidation. Front. Microbiol. 6 https://doi.org/10.3389/fmicb.2015.00484.
Kleerebezem, R., Loosdrecht, M.C.M., 2010. A Generalized Method for Thermodynamic State Analysis of Environmental Systems A Generalized Method for Thermodynamic 37–41. https://doi.org/10.1080/10643380802000974.
Kleerebezem, R., Mendez, R., 2002. Autotrophic denitrification for combined hydrogen sulfide removal from biogas and post-denitrification. Water Sci. Technol. 45, 349–356.
Lagarias, J.C., Reeds, J.A., Wright, M.H., Wright, P.E., 1998. Convergence properties of the nelder–mead simplex method in low dimensions. SIAM J. Optim. 9 https://doi.org/10.1137/S1052623496303470.
Lan, L., Zhao, J., Wang, S., Li, X., Qiu, L., Liu, S., Bin Nasry, A.A.N., 2019. NO and N2O accumulation during nitrite-based sulfide-oxidizing autotrophic denitrification. Bioresour Technol Rep 7. https://doi.org/10.1016/j.biteb.2019.100190.
Li, W., Liu, J., Sui, X., Lin, M., Zhao, W., Zhen, Y., Bing, X., Lin, J., 2021. Response of the reactor performances and bacterial communities to the evolution of sulfide-based mixotrophic denitrification processes from nitrate-type to nitrite-type. Biochem. Eng. J. 173 https://doi.org/10.1016/j.bej.2021.108069.
Li, Y., Han, Q., Li, B., 2023. Engineering-scale application of sulfur-driven autotrophic denitrification wetland for advanced treatment of municipal tailwater. Bioresour. Technol. 379 https://doi.org/10.1016/j.biortech.2023.129035.
Lin, S., Mackey, H.R., Hao, T., Guo, G., Loosdrecht, M.C.M., Chen, G., 2018. Biological sulfur oxidation in wastewater treatment: a review of emerging opportunities. Water Res. https://doi.org/10.1016/j.watres.2018.06.051.
Lu, H., Huang, H., Yang, W., Mackey, H.R., Khanal, S.K., Wu, D., Chen, G.H., 2018. Elucidating the stimulatory and inhibitory effects of dissolved sulfide on sulfur-oxidizing bacteria (SOB) driven autotrophic denitrification. Water Res. 133, 165–172. https://doi.org/10.1016/j.watres.2018.01.022.
Madigan, M.T., Bender, K.S., Buckley, D.H., Sattley, W.M., Stail, D.A., 2019. Brock Biology of Microorganisms, fifteenth ed. Pearson Education Limited.
Mannucci, A., Munz, G., Mori, G., Lubello, C., 2012. Biomass accumulation modelling in a highly loaded biotrickling filter for hydrogen sulphide removal. Chemosphere 88, 712–717. https://doi.org/10.1016/j.chemosphere.2012.04.026.
Mora, M., Dorado, A.D., Gamisans, X., Gabriel, D., 2015a. Investigating the kinetics of autotrophic denitrification with thiosulfate: modeling the denitritation mechanisms and the effect of the acclimation of SO-NR cultures to nitrite. Chem. Eng. J. 262, 235–241. https://doi.org/10.1016/j.cej.2014.09.101.
Mora, M., Fernández, M., Gómez, J.M., Cantero, D., Lafuente, J., Gamisans, X., 2015b. Kinetic and Stoichiometric Characterization of Anoxic Sulfide Oxidation by SO-NR Mixed Cultures from Anoxic Biotrickling Filters 77–87. https://doi.org/10.1007/s00253-014-5688-5.
Mora, M., Guisasola, A., Gamisans, X., Gabriel, D., 2014. Examining thiosulfate-driven autotrophic denitrification through respirometry. Chemosphere 113, 1–8. https://doi.org/10.1016/J.CHEMOSPHERE.2014.03.083.
Polizzi, C., Gabriel, D., Munz, G., 2022. Successful sulphide-driven partial denitrification : efficiency , stability and resilience in SRT-controlled conditions. Chemosphere 295, 133936. https://doi.org/10.1016/j.chemosphere.2022.133936.
Quaglio, M., Fraga, E.S., Galvanin, F., 2018. Chemical Engineering Research and Design Model-based design of experiments in the presence of structural model uncertainty : an extended information matrix approach. Chem. Eng. Res. Des. 136, 129–143. https://doi.org/10.1016/j.cherd.2018.04.041.
Reichert, P., Vanrolleghem, P., 2001. Identifiability and uncertainty analysis of the river water quality model No. 1 (RWQM1). Water Sci. Technol. 43 https://doi.org/10.2166/wst.2001.0442.
Rittmann, B.E., McCarty, P.L., 2001. Environmental Biotechnology: Principles and Applications, first ed. McGraw-Hill Education, New York.
Roels, J.A., 1983. Energetics and Kinetics in Biotechnology. Elsevier Biomedical Press, Amsterdam.
Sahinkaya, Erkan., Dursun, Nesrin., Kilic, Adem., Demirel, Sevgi., Uyanik, Sinan., Cinar, Ozer., 2011. Simultaneous heterotrophic and sulfur-oxidizing autotrophic denitrification process for drinking water treatment : control of sulfate production. Water Res. 45 (20), 6661–6667. https://doi.org/10.1016/j.watres.2011.09.056.
Savageau, M.A., 1984. Energetics and kinetics in biotechnology. J. A. Roels. Q Rev Biol 59, 179. https://doi.org/10.1086/413814.
Sublette, Kerry L., Sylvester, Nicholas D., 1987. Of natural gas. Biotechnol. Bioeng. XXIX: , 57–249.
Wang, K., Qaisar, M., Chen, B., Liu, S., Wu, Y., Zheng, Z., Cai, J., 2022. Strategy for rapid recovery of simultaneous sulfide and nitrite removal under high substrate inhibition. Biochem. Eng. J. 180 https://doi.org/10.1016/j.bej.2022.108368.
Wang, L., Liu, J., Li, Y., Liu, Z., Zhang, L., Che, H., Cui, H., Zhang, Y., 2023. Elemental sulfur-driven autotrophic denitrification process for effective removal of nitrate in mariculture wastewater: performance, kinetics and microbial community. Chemosphere 337, 139354. https://doi.org/10.1016/j.chemosphere.2023.139354.
Wu, D., Ekama, G.A., Chui, H.K., Wang, B., Cui, Y.X., Hao, T.W., van Loosdrecht, M.C.M., Chen, G.H., 2016. Large-scale demonstration of the sulfate reduction autotrophic denitrification nitrification integrated (SANI®) process in saline sewage treatment. Water Res. 100, 496–507. https://doi.org/10.1016/j.watres.2016.05.052.
Xu, X., Chen, C., Wang, A., Guo, W., Zhou, X., Lee, D., Ren, N., Chang, J., 2014. Simultaneous removal of sulfide , nitrate and acetate under denitrifying sulfide removal condition : modeling and experimental validation. J. Hazard Mater. 264, 16–24. https://doi.org/10.1016/j.jhazmat.2013.10.056.
Xu, G., Yin, F., Chen, S., Xu, Y., Yu, H.Q., 2016. Mathematical modeling of autotrophic denitrification (AD) process with sulphide as electron donor. Water Res. 91, 225–234. https://doi.org/10.1016/j.watres.2016.01.011.
Yavuz, B., Türker, M., Engin, G.Ö., 2007. Autotrophic removal of sulphide from industrial wastewaters using oxygen and nitrate as electron acceptors. Environ. Eng. Sci. 24 https://doi.org/10.1089/ees.2006.0068.
Zhang, D., Cheng, L., Zhang, S., Zheng, J., 2023. Denitrification performance and microbial community analysis of sulfur autotrophic denitrification filter for low-temperature treatment of landfill leachate. J. Environ. Chem. Eng. 11 https://doi.org/10.1016/j.jece.2023.109314.
Zhou, Y., Oehmen, A., Lim, M., Vadivelu, V., Ng, W.J., 2011. The role of nitrite and free nitrous acid (FNA) in wastewater treatment plants. Water Res. 45, 4672–4682. https://doi.org/10.1016/j.watres.2011.06.025.